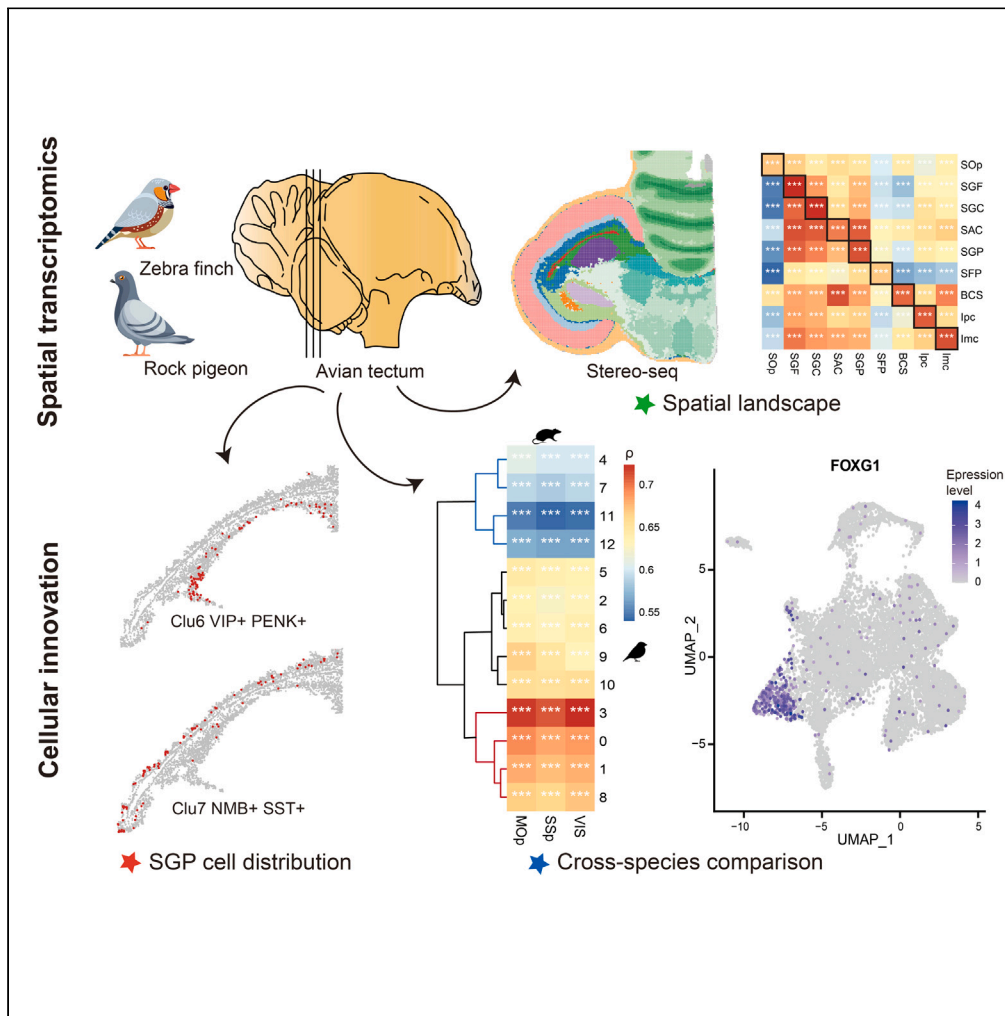


Article

Spatial and single-nucleus transcriptomics decoding the molecular landscape and cellular organization of avian optic tectum



Kuo Liao, Ya Xiang, Fubaoqian Huang, ..., Zhenlong Wang, Shiping Liu, Zhenkun Zhuang

chenduoyuan@genomics.cn (D.C.)
wzl@zzu.edu.cn (Z.W.)
liushiping@genomics.cn (S.L.)
zhuangzhenkun@genomics.cn (Z.Z.)

Highlights

Stereo-seq constructs the spatial molecular map of avian OT

Spatial landscape reveals layer-specific signatures and functional pathways of OT

SGP is the pivotal layer associated with advanced functions in avian OT

A population of cells highly expressing FOXG1 emerges in avian OT



Article

Spatial and single-nucleus transcriptomics decoding the molecular landscape and cellular organization of avian optic tectum

Kuo Liao,^{1,2} Ya Xiang,^{2,3} Fubaoqian Huang,^{1,2} Maolin Huang,⁴ Wenbo Xu,⁴ Youning Lin,^{2,5} Pingfang Liao,^{2,6} Zishi Wang,⁴ Lin Yang,⁴ Xinmao Tian,⁴ Duoyuan Chen,^{2,5,*} Zhenlong Wang,^{4,*} Shiping Liu,^{2,5,*} and Zhenkun Zhuang^{2,5,7,*}

SUMMARY

The avian optic tectum (OT) has been studied for its diverse functions, yet a comprehensive molecular landscape at the cellular level has been lacking. In this study, we applied spatial transcriptome sequencing and single-nucleus RNA sequencing (snRNA-seq) to explore the cellular organization and molecular characteristics of the avian OT from two species: *Columba livia* and *Taeniopygia guttata*. We identified precise layer structures and provided comprehensive layer-specific signatures of avian OT. Furthermore, we elucidated diverse functions in different layers, with the stratum griseum periventriculare (SGP) potentially playing a key role in advanced functions of OT, like fear response and associative learning. We characterized detailed neuronal subtypes and identified a population of *FOXP1+* excitatory neurons, resembling those found in the mouse neocortex, potentially involved in neocortex-related functions and expansion of avian OT. These findings could contribute to our understanding of the architecture of OT, shedding light on visual perception and multifunctional association.

INTRODUCTION

As one of the most crucial sensory information transmission hubs, the optic tectum (OT), which is known as superior colliculus (SC) in mammals, performs a diverse array of functions in vertebrates.^{1–3} It plays a significant role in visual information processing, eye movement, fear response, and even prey capture activity.^{3,4} In addition to its involvement in the transformation of multiple visual inputs, the deeper layers of the OT also can receive inputs from somatosensory and auditory sources, facilitating the alignment of various sensory neural maps and contributing to certain motor functions.^{5–7} And most recently, OT has been reported to play a role in higher cognitive functions such as selective attention and decision-making.^{8–10} Meanwhile, OT or SC is one of the most conservative structures during vertebrate brain evolution.³ From the lamprey to primates, OT has formed and existed for millions of years, while still exhibiting striking similarities in its fundamental functions, layered organization, and cellular composition.¹¹

In fish, OT located in the midbrain constitutes a substantial portion of the brain, serving as the main visual center where the majority of optic fibers terminate.¹² During evolution, the OT has gradually developed a layered structure exhibiting enhanced clarity and precision. In birds, which possess an exceptional visual capability, the OT has expanded and developed into the most intricate and distinct laminar structure in all vertebrates, containing about 15 detailed layers.^{3,13} This highly expanded OT plays a very important role in diverse functions of birds, including some higher processes, like attention and cognition. However, in mammals, the advent of the forebrain has brought about a shift in the primary visual processing tasks to the primary visual cortex (V1).^{14,15} As a consequence, only a few visual-related functions and some instinctive reactions are still kept in the SC.^{1,16,17} Despite numerous studies conducted on the functional research of the SC in mice or monkeys, the driving factors behind this evolutionary transformation have received limited attention and remain elusive. Furthermore, gaining a comprehensive understanding of this fundamental function transition may provide us with a fresh perspective to explore the reasons for neocortex expansion in mammals or primates.

Previous investigations into the structure and function of OT have predominantly relied on anatomical and electrophysiological approaches or have focused only on limited molecular markers. Consequently, our ability to form a comprehensive and in-depth understanding

¹School of Biology and Biological Engineering, South China University of Technology, Guangzhou 510006, China

²BGI Research, Hangzhou 310030, China

³College of Life Sciences, Northwest University, Xi'an 710069, China

⁴School of Life Sciences, Zhengzhou University, Zhengzhou 450001, China

⁵BGI Research, Shenzhen 518083, China

⁶College of Life Sciences, University of Chinese Academy of Sciences, Beijing 100049, China

⁷Lead contact

*Correspondence: chenduoyuan@genomics.cn (D.C.), wzl@zzu.edu.cn (Z.W.), liushiping@genomics.cn (S.L.), zhuangzhenkun@genomics.cn (Z.Z.)
<https://doi.org/10.1016/j.isci.2024.109009>



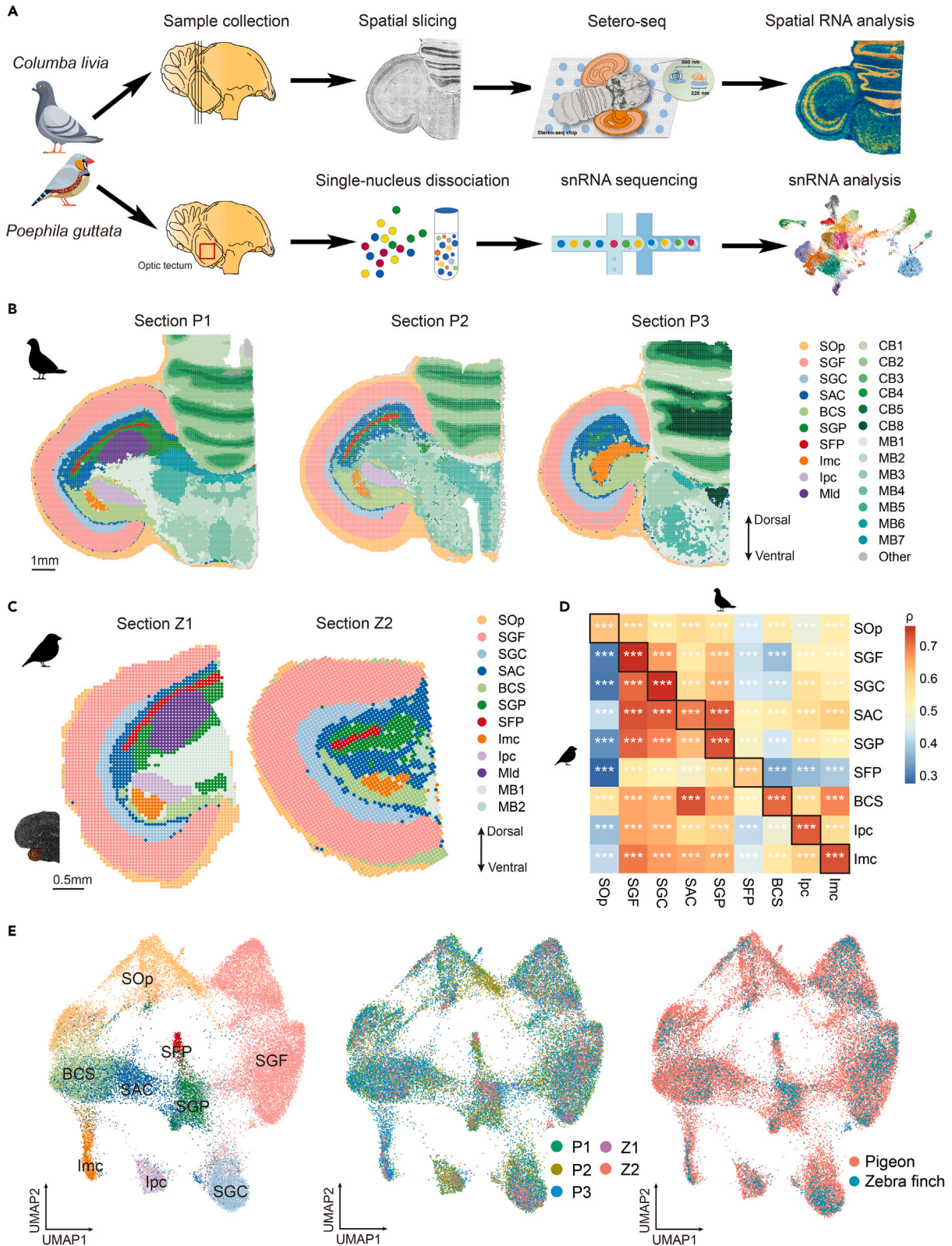


Figure 1. The experimental design and spatial landscape of avian tectum

(A) Schematic workflow of the study.

(B) The unsupervised clustering and main annotation of the pigeon sections. Bin100 as a unit. SOp, stratum opticum; SGF, stratum griseum et fibrosum superficiale; SGC, stratum griseum centrale; SAC, stratum album centrale; SGP, stratum griseum periventriculare; SFP, stratum fibrosum periventriculare; BCS, brachium colliculi superioris; Mld, nucleus mesencephalicus lateralis pars dorsalis; lmc, nucleus isthmi pars magnocellularis; lpc, nucleus isthmi pars parvocellularis; MB, midbrain; CB, cerebellum. Section P1, P2, and P3 were from the position at 12.0, 12.5, and 13.0 mm from the forebrain extremity along the anterior-to-posterior direction respectively.

(C) The unsupervised clustering and main annotation of the zebra finch sections. Bin100 as a unit. Section Z1 and Z2 were from the position at 6.5 and 6.0 mm from the forebrain extremity.

(D) The correlation of main OT regions between zebra finch and pigeon. ρ : Spearman correlation coefficient.

(E) Uniform manifold approximation and projection (UMAP) plot of integrated bins from all sections, which only contains the main tectum regions.

of OT at the cellular and molecular levels has been restricted. Meanwhile, despite the abundant functions of OT, the precise neural mechanisms underlying these functions remain poorly defined.⁴ Past studies have revealed that the neural network and circuits of OT are the main contributors to its processing and analysis.^{18,19} At the cellular level, glutamatergic projection neurons in OT are reported to encode distinct sensorimotor transformations for fear response, prey catching, and predator avoidance, while the γ -aminobutyric acid (GABA) neurons are related to eye movement for selective attention and wakefulness.⁴ However, the precise laminar distribution of these neural cells is still unclear. Moreover, our understanding of the subtypes of main neurons and their characteristics remains relatively rudimentary. To have a deeper insight into these functional neural mechanisms and evolution transitions in OT, we are encouraged to develop a more comprehensive and precise landscape of OT. Here, we employed an omics-based approach, incorporating high-resolution spatial transcriptomic sequencing and single-nucleus RNA sequencing (snRNA-seq), to generate a spatially resolved transcriptomic atlas of avian OT. Particularly, based on the comparison between birds and mice, we proved the polyfunctional potential of OT in birds and explained its mechanism at the cellular level.

RESULTS**Spatial landscape of avian tectum**

To build up a spatial transcriptomic landscape of the OT, here we utilized the spatial enhanced resolution omics sequencing (Stereo-seq)²⁰ on the OT of two species of birds: pigeon (*Columba livia*) and zebra finch (*Taeniopygia guttata*). After the sample collection and Stereo-seq, we collected three sections from pigeons and two from zebra finches at adjacent positions (Figure 1A). The Stereo-seq is based on the DNA nanoball (DNB)-patterned arrays, of which the diameter is 220 nm and the spacing is 500 nm. Thus, to obtain better quality for the subsequent unsupervised clustering and analysis, we first adopted a binning strategy with a bin size of 100 (bin; 100 × 100 DNBs, 50 μ m diameter), similar to previous studies.²⁰ After the quality control (QC), the average number of unique molecular identifiers (UMIs) detected per bin on all sections was around 5,400 with more than 1,600 genes detected (Figure S1A and S1B).

To delineate the transcriptional spatial organization of the OT, we applied an unsupervised clustering method based on graph convolutional network (GCN) on our all sections with SpaGCN.²¹ All sections were clustered into a minimum of nine distinct sub-layers, which demonstrated the intricate layered structure of avian OT at the transcriptomic level (Figures S1C and S1D). Here, we annotated our sections into corresponding main layers, based on the acknowledged anatomical structure and unsupervised clustering results¹³ (Figures 1B and 1C). From the superficial to the deep layers, the labeled OT layers were as follows: the stratum opticum (SOp), the stratum griseum et fibrosum superficiale (SGF), the stratum griseum centrale (SGC), the stratum album centrale (SAC), the stratum griseum periventriculare (SGP), and the stratum fibrosum periventriculare (SFP) (Figure 1B). In addition to these layers, there were two crucial components of the nucleus isthmi, the pars magnocellularis (lmc) and pars parvocellularis (lpc). Referring to the unsupervised clustering results, we integrated the regions surrounding the lpc and lmc into the brachium colliculi superioris (BCS). Besides these visually related regions, we also successfully captured and discerned the nucleus mesencephalicus lateralis pars dorsalis (Mld), which is beneath the OT and participates in the audition of non-mammal vertebrates.²² In this study, we did not extensively elucidate other midbrain (MB) or cerebellum (CB) regions; however, their locations were also well aligned with existing knowledge of corresponding anatomical regions in birds and may provide valuable insights for future research endeavors. Especially, to mark the *in situ* distribution of individual cells on the section, we performed single-stranded DNA (ssDNA) staining to highlight the nucleus before next-generation sequencing, which can reflect the cell density of the OT and was in line with our spatial annotation (Figures S1E). From the transcriptional level, we could also prove that avian OT was highly conserved between different species (Figure 1D).

To further control the batch effect, we clustered and annotated five sections from different spatial positions independently and integrated them with their weighted-nearest neighbors²³ (Figures 1E and S1F). The integration results showed fine alignment of five spatial sections despite they were sampled from different samples and positions, which further demonstrated the accuracy of our methodology and annotation. All regions of OT possessed unique characteristics. Notably, from the uniform manifold approximation and projection (UMAP) visualization, we observed that a part of SAC shared similarities with the BCS, which was also reasonable for their location in the same layer depth (Figure 1E). In conclusion, here we provided a comprehensive spatial landscape of the avian OT in two species and then reconstructed its laminar distribution with transcriptome for the first time.

Layer-specific signatures of avian OT

In order to discover the layer-specific features of each region in avian OT, we conducted a differential expression analysis between them with the integrated data from pigeons and zebra finches (Figure 2A and Table S1). Moreover, we visualized part of these region-specific markers in

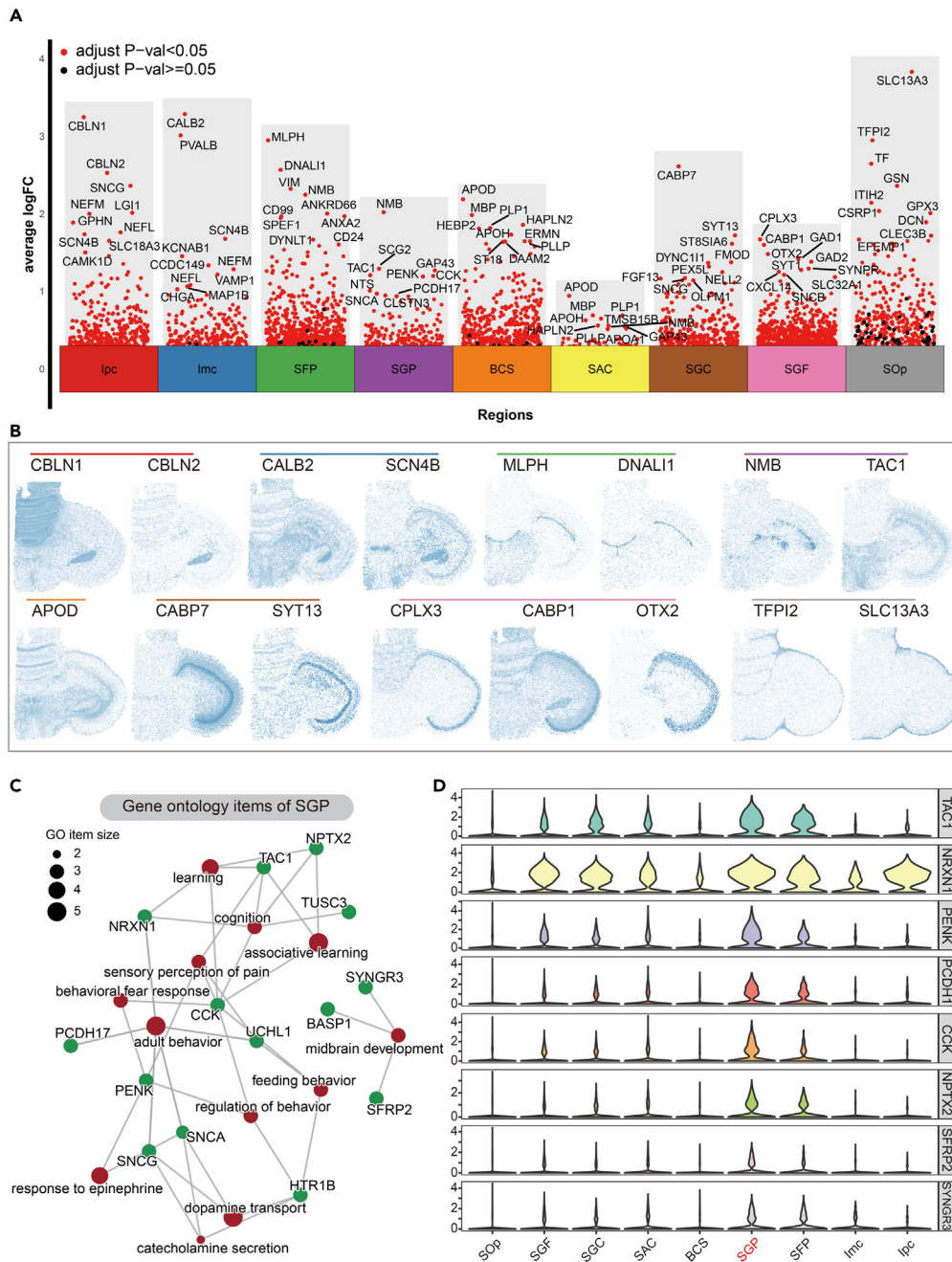


Figure 2. Molecular characteristics of avian OT

(A) Volcano plot showing highly differentially expressed genes of regions by Wilcoxon Rank-Sum test. Adjust p value by Benjamini and Hochberg (BH) method. Only the top 10 genes were marked except for unknown transcripts in the genome.

(B) Spatial feature plots showing the expression of representative markers selected from (A). Section P1 was shown here.

(C) Selected GO items (red) and enriched genes (green) of the SGP. The q value of all items selected was less than 0.05. Genes were top 50 DEGs of SGP compared with other regions of OT, of which the adjusted p value was less than 0.05.

(D) Stacked violin plot showing the expression level of genes from Figure (C) in main optic regions.

our spatial section D6, which further confirmed their regional expression patterns (Figure 2B). Among differentially expressed genes (DEGs), two homologous cerebellins, *CBLN1* and *CBLN2*, were enriched in the lpc. The cerebellin family is known to play a significant role in synapse development and function,^{24,25} suggesting the wide connection between lpc and other regions. Meanwhile, we found high expression levels of calbindin 2 (*CALB2*) in the lmc region, which has also been reported as enriched in the retina, lmc, and nucleus retundus (Rt) of chickens

before.²⁶ Additionally, two calcium binding proteins, *CABP7* and *CABP1*, were respectively highly expressed in the SGF and SGC, which are the two main layers involved in receiving information from the retina. The calcium binding protein family was reported expressed in the amacrine cells and cone bipolar cells of the retina before, and they are important for the normal transmission of light responses in mammals.²⁷ Our findings in birds underscore their significance as well. The complexin 3 (*CPLX3*) has a similar importance in the visual system,²⁸ which was found enriched in the SGF. Through these important proteins in the visual system, we can observe the conservation between birds and mammals in terms of visual signal transmission. And with the expressed pattern, we could confirm the regions, like SGF and SGC, which directly accept the retina input at the gene expression level. Moreover, we found that the neuromedin B (*NMB*) was enriched in the deeper layers of OT, including SGP and SFP, which is commonly released in the pain- and itch-sensing somatosensory neurons.^{29,30} Besides the *NMB*, the neurotensin (*NTS*) also stood out in the SGP, which is related to numerous biological processes, including pain sensation.³¹ Hence, our findings further support the multifunctional capability of the SGP in different sensory processes, and these results first shed light on the potential regulatory mechanisms of OT in processing multimodal information.

Through the layer comparison, we identified and presented the overall region-specific markers of OT, which held significant potential for functional investigations for different layers. Hence, to further clarify the functional specialization of OT, we conducted the gene ontology (GO) enrichment analysis on top DEGs of each domain (Figure S2A). Through the GO, it was found pathways enriched in the SFP, which is located around the ventricle, were mainly about the cilium organization and assembly, as well as the extracellular transport. This suggested its function of facilitating cerebrospinal fluid flow and substance transfer with the ventricle. Consistent with the UMAP results (Figure 1E), the GO items enriched in the SAC and BCS showed a lot of similarities. They are both highly related to the glial cell development and myelination of axons. Additionally, as the main visual transition and processing layer, the SGF was found to focus on synaptic formation and neural signal conduction by the enrichment of DEGs (Figure S2A).

Intriguingly, as for the SGP, we found it possessed the most diverse functions, including some advanced processes, like fear response, associative learning, cognition, and adult behaviors (Figure 2C). It has been broadly proved that OT or SC is associated with fear response and predator avoidance in vertebrates.³ Hence, here we not only further confirmed these abilities of OT but also identified SGP as the main center of these behaviors in OT. In addition, it has been reported the sensitive response to epinephrine and dopamine may be related to stress reaction in creatures,^{32,33} which may also explain the mechanism of SGP to react rapidly when facing danger in birds here (Figure 2C). Related genes of response to epinephrine and dopamine, like *PENK*, *SNCG*, and *HTR1B*, were found to be highly expressed in the deep layers of OT (Figure 2C). Other advanced function related genes, like *TAC1*, *NRXN1*, *PCDH1*, *CCK*, and *NPTX2*, were revealed to be enriched in SGP as well (Figures 2C and 2D). Moreover, except for these higher functions of SGP, the midbrain development related genes, like *SFRP2* and *SYNGR3*,^{34,35} were also mainly enriched in the deeper layers of OT, including SGP and SFP, which indicated they may be the key layers involved in the significant expansion of avian OT (Figures 2C and 2D).

Collectively, through the Stereo-seq, we first systematically provided the spatial transcriptional landscape of avian OT and revealed the differentially enriched genes of each layer. Based on this, we further reinterpreted the molecular and functional characteristics of various anatomical regions of OT from the molecular level. The spatial landscape of OT at the transcriptional level provided a cellular substrate that could contribute to the anatomical layer elucidation and visual evolution analysis in the future.

Neurotransmitter expression patterns reveal potential neural connections within avian OT

Neurotransmitters are mediators of electrical and chemical communication in the brain, which plays a critical role in facilitating normal nerve function and orchestrating complex biological activities. To elucidate the topography of gene expression profiles of known neurotransmitter receptors and transporters in OT (Table S2), we employed a module-scoring approach using our spatial data.^{36–43} This approach involved scoring the expression levels of key categories of nerve transport and receptor genes, including GABA, glutamate, monoamine, and acetylcholine (Figures S3A and S3B). As anticipated, GABA and glutamate were the main neurotransmitters in the visual processing of OT, as the superficial layers of OT undertook the most signal transmission tasks.⁴⁴ Particularly, compared with the close acceptance level of glutamate and GABA, neurons in OT seemed to mainly rely on GABA to deliver signals to other neurons or brain regions (Figures S3A and S3B). Likewise, for the monoamine neurotransmitter, here we took 5-hydroxytryptamine (5-HT) as an example, certain midbrain regions were the main efferent nerves as reported.⁴⁵ The broad distribution of 5-HT receptors in OT indicated OT worked as one of the specific output targets from other midbrain subregions (Figure S3B). Furthermore, the release of acetylcholine was significantly centered around the *Ipc*, while the receptors were dispersed in the SGP, SAC, SGC, and SGF, which was in line with previous studies.⁴⁶ The acetylcholine transmission of *Ipc* to other OT regions has been revealed an important role in selective attention before.^{47,48} To summarize, here we depicted comprehensively the receptors and transporters distribution of four main neurotransmitters (GABA, glutamate, monoamines, and acetylcholine) within the OT of pigeon for the first time. Particularly, some of them, like the 5-HT, are barely reported by previous studies. These results offered a more intensive understanding of potential neural connections existing in the avian brain, helping us to understand the communication that existed between OT and other brain regions.

Spatial cellular diversity of avian tectum

Although using bins as units is a common approach in spatial omics analysis for region clustering nowadays, it should be noted that a divided bin still only represents a delineated boundary rather than an individual cell.^{20,49} To obtain the spatial cellular organization of OT, we applied a watershed-based approach to segment single cells from the spatial section referring to its ssDNA staining, which was conducted by Spateo⁵⁰ (Figure 3A). Notably, since the cells of the avian brain are much smaller than normal mammalian cells, it is quite difficult to obtain high-quality

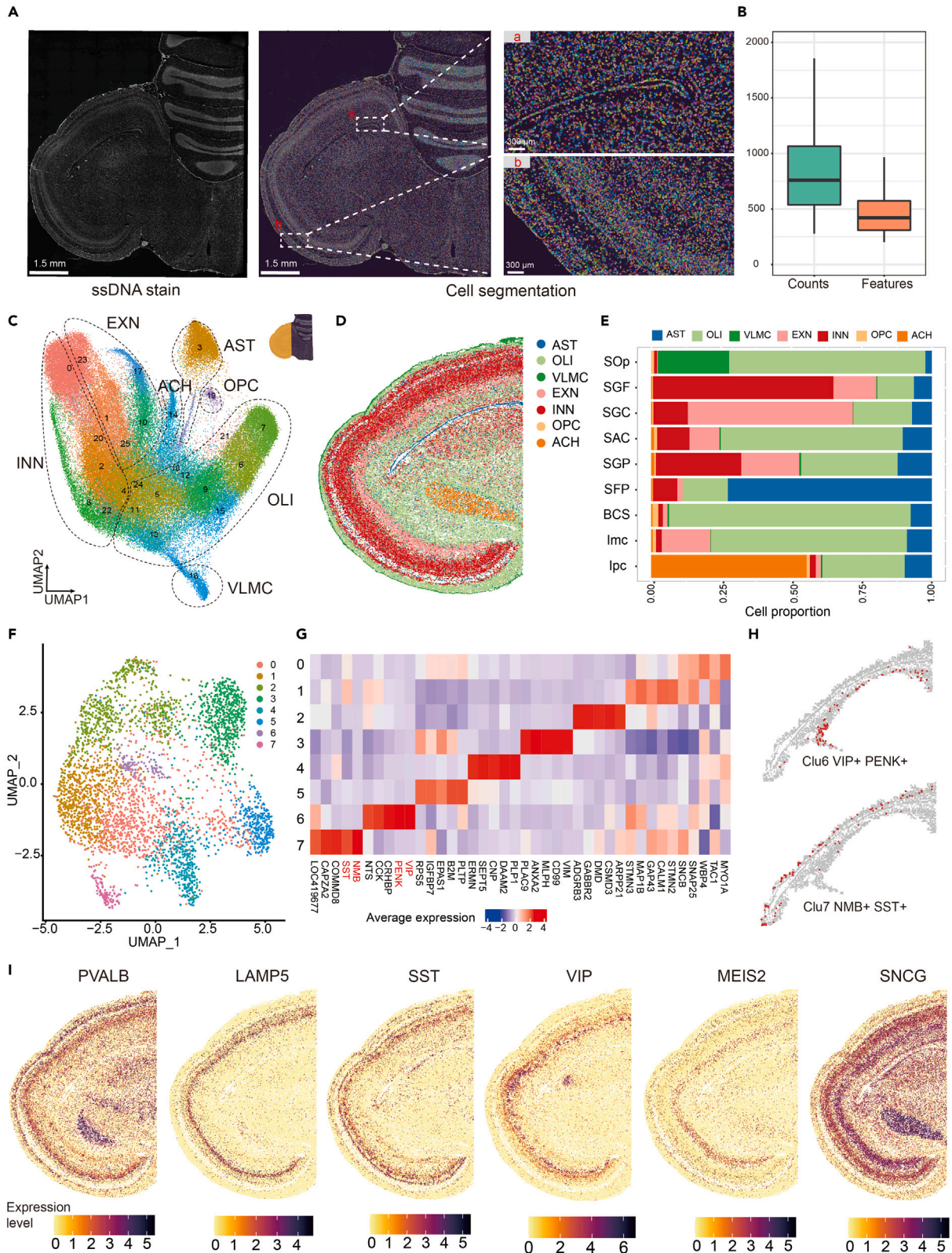


Figure 3. Spatially segmented cells of avian OT

- (A) ssDNA staining of OT section (Left) and spatially assigned nuclei by Spateo (Median). Corresponding nucleus areas were properly expanded to include the cytoplasm. Zoom in segmented cells (Right).
- (B) Boxplot of genes (Left) and counts (Right) number of segmented cells. Only the main tectum regions were contained.
- (C) UMAP showing the unsupervised clustering of segmented cells. EXN, excitatory neurons; INN, inhibitory neurons; OLI, oligodendrocytes; AST, astrocytes; OPC, dendrocyte precursor cells; VLMC, vascular leptomeningeal cells; ACH, acetylcholinergic neurons.
- (D) Spatial plot of identified cell types.
- (E) Bar plot showing cell type proportion of each region.
- (F) Sub-clustering of the cells from SGP and SFP.
- (G) Heatmap of top 5 DEGs of each subcluster from SGP and SFP.
- (H) Distribution of Clu6 *VIP+PENK+* cells (Up) and Clu7 *NMB+SST+* cells (Down).
- (I) Expression levels of classic INN markers on space, including *PVALB*, *LAMP5*, *SST*, *VIP*, *MEIS2*, and *SNCG*.

data at cellular resolution with existing technology nowadays. Therefore, here we only segmented and clustered section P1, which had the highest quality in all sections. For subsequent analysis, we focused exclusively on the integral part of the tectum. After filtering out the low-quality cells, we obtained 89,521 segmented cells, with an average of 782 UMIs and 421 genes per cell (Figure 3B).

Upon dimension reduction and clustering, we annotated these cells into six major cell types based on known markers for neural cells^{51–53}: excitatory neurons (EXN; *SLC17A6+*), inhibitory neurons (INN; *GAD2+*), oligodendrocytes (OLI; *PLP1+*), astrocytes (AST; *AQP4+*), dendrocyte precursor cells (OPC; *OLIG2+*), vascular leptomeningeal cells (VLMC; *DCN+*), and acetylcholinergic neurons (ACH; *SLC18A3+*) (Figures 3C and S4A). OLI were found to be the predominant cell type in the OT, which was consistent with previous reports.⁵⁴ This observation may be attributed to the high-density distribution of long axons and synapses of OT. Moreover, after embedding the segmented cells back into their spatial context, we observed distinct cell distribution patterns of domains in OT (Figures 3D and 3E). As the superficial layer of the midbrain, the SOp exhibited a higher abundance of VLMC and OLI. The SFP layer had the most AST, which was in line with the expected distribution around the ventricles, as AST-like cells were commonly found near the ventricular regions in many vertebrates.⁵⁵ Regarding neuron types, the SGP showed enrichment of INN, while the SGC was enriched with EXN, consistent with previous studies.⁵⁶ Particularly, as reported before, the major cell type in lpc was CHN.⁴⁶ Collectively, the fine alignment between the distribution of these segmented cells and previous experimental research further proved the accuracy of our cell segmentation and annotation. Meanwhile, compared with previous studies, which were mainly based on histochemical staining of one or two genes, here we provided a more precise and comprehensive OT organization of all cell types by spatial omics.

To have an in-depth understanding of OT in processing diverse information, we then first focused on SGP (SPF included) and identified distinct eight subclusters of cells in it (Figure 3F). In all subclusters of SGP, we noticed two special populations of cells with significantly high expression of *VIP/PENK* (Clu6) and *NMB/SST* (Clu7), respectively (Figure 3G). These genes were relevant to advanced brain functions, like associative learning, and showed distinct enrichment in the avian SGP (Figure 2C). The Clu6 cells were found to highly express *CCK* and *NTS* as well, and *CCK+* neurons have been reported to be highly related to the fear response in creatures.^{57,58} Benefiting from the cellular resolution of Stereo-seq, here we could ascertain major cell populations involved in the complex functions of SGP and further delineate their spatial distribution traits. Notably, we found these two cell types (Clu6 *VIP+PENK+* and Clu7 *NMB+SST+*) were differentially distributed in space (Figure 3H). The Clu6 *VIP+PENK+* cells were mainly distributed in the medial, while Clu7 *NMB+SST+* cells preferred to exist in the lateral SGP. The conspicuous enrichment of Clu6 interposed between the SGP and Mld may also suggest their involvement in the process of visual and auditory integration occurring within the OT region. These observations warrant our further investigation through prospective experimental studies.

Besides the integration of multi-modal signals in OT, the detailed subtypes of INN in OT and their distribution have also remained unclear in past studies.⁴ To address this, here we used classic markers of INN in mammals to clarify their spatial distribution in OT, which included *PVALB*, *LAMP5*, *SST*, *VIP*, *MEIS2*, and *SNCG*. Generally, we found the distribution of typical INN subtypes further possessed a precise layer structure, not in random or pillar distribution, which was quite an interesting result (Figure 3I). Specifically, in the avian OT, the *PVALB+* cells were mainly located around the outer layers, followed by the *LAMP5+*, *SST+*, *VIP+*, and *MEIS2+* cells. This delicate structure of OT may play an important role in the processing and projection of different visual information input of OT and help to form a visual map. Besides outer layers, the lmc was also found to enrich with *PVALB+* cells, which was consistent with past reports.⁵⁹ On the contrary, the lpc was observed to have plentiful *SNCG+* cells. This difference between the two nucleus isthmi was quite interesting and worthy of further attention. We also observed a similar distribution pattern of various INN subtypes in the segmented section of zebra finch, which underscored the remarkable conservation of this precise layer structure in the tectum across avian species (Figure S4B). To substantiate the uniqueness of this structure in birds, we compared the gene expression patterns with those found in the SC using transcriptional spatial data from mouse brains,⁶⁰ and checked the *in situ* hybridization (ISH) data of mice in Allen Brain Atlas (ABA). It turned out that this precise structure of INN was not present by SC of mice, further highlighting the sophisticated nature of the avian OT (Figures S4C and S4D). Meanwhile, compared with the SC, we found that *PVALB+* neurons were abundant in both OT and SC, while the *SNCG+* neurons were only enriched in OT (Figure S4D).

In summary, in this part, we further explored the OT at spatial cellular resolution and provided its cell distribution landscape. We identified two pivotal cell populations in the SGP and delineated their distinct anatomical spatial distribution. Additionally, our findings described a highly precise architecture of interneurons within the avian tectum region, surpassing that of the mouse SC. Given previously, these findings provided us with new insights into the intricate organization and functional specialization of the OT at a cellular resolution.

Single-cell atlas of the deep layers of OT

The deep layers of OT (dOT) or SC are associated with the processing of vision, auditory, and somatosensory.⁴ Meanwhile, it's reported to be involved in some motor functions and the visual and auditory alignment.⁵ In our previous analysis, we proved the fear response and associative learning abilities of OT, especially in the dOT, at the transcriptional level. Therefore, to have a more profound understanding of the dOT and further elucidate its function mechanisms, we applied snRNA-seq on the dOT from two adult zebra finches (Figures 1A, S5A, and S5B). After QC, we obtained 29,281 single-nuclei transcriptomes and identified seven major populations of neuronal and nonneuronal cells (Figure 4A). Like before, referring to well-established marker genes,^{51–53,61} we annotated clusters of excitatory neurons (EXN; *SLC17A6+*), inhibitory neurons (INN; *GAD2+*), oligodendrocytes (OLI; *PLP1+*), astrocytes (AST; *SLC1A2+*), dendrocyte precursor cells (OPC; *PDGFRA+*), microglial cells (MIC; *C1QB+*), and blood cells (*HBAD+*) (Figure 4B).

We mainly focused on the 23,514 neurons in our single-cell data. To gain insights into the cellular and molecular mechanisms underlying the exceptional abilities of avian dOT, we first subclustered the EXN from our data and identified 11 subclusters of EXN, which indicated the presence of diverse EXN populations in dOT and highlighted the high density of excitatory neurons in this region (Figure 4C). Given the involvement of dOT in visual, somatosensory, and motor functions,⁴ we compared our data with an atlas of single-cell data from three major mouse brain regions: the visual area (VIS), primary somatosensory area (SSp), and primary motor area (MOp).⁶² By examining the gene expression correlations, we found varying degrees of similarity between the EXN clusters in OT and the neocortical regions. The EXN_0, EXN_1, EXN_3, and EXN_8 (group 1) exhibited higher correlation with the neocortex, while EXN_4, EXN_7, EXN_11, and EXN_12 (group 2) had much less similarity (Figure 4D). Especially, the difference of correlation across neocortex regions was minimal. Based on this observation and background knowledge, we hypothesized these cell populations with high similarity with mouse neocortex may play a more important role in advanced functions. To further explore the difference between the two groups of EXN, we perform a differential expression analysis between them (Figure 4E). The group 1 EXN was found to highly express *LOC116808653*, the glutamate ionotropic receptor AMPA type subunit 1 (*GRIA1*), and neural cell adhesion molecule L1-like protein (*CHL1*). Upregulated DEGs of group 1 were mainly related to the synaptic transmission, synapse organization, and axon development pathways (Figure 4F). Besides, based on this GO enrichment result, EXN in group 1 appeared to be more related to cognitive, learning, and memory, which then supported our initial hypothesis. Specifically, we then focused on the EXN_3, which exhibited the highest correlation with mouse EXN. The EXN_3 was marked by the forkhead box G1 (*FOXP1*), which is a key transcription factor for the vertebrate to expand the forebrain and acquire higher order information processing abilities⁶³ (Figure 4G). The existence of *FOXP1+* cells in the OT of zebra finch was verified by our spatial data (Figure S5D). Additionally, to validate the specificity of these neurons in OT, we examined the expression of *FOXP1* in mouse brains with ISH data from ABA and found it was predictably present in the neocortex but vacant in the mammalian SC (Figure S5E). This further indicated that *FOXP1+* neurons were unique to avian OT and not present in the mammalian SC. We assumed that the absence of *FOXP1* in the midbrain may be related to the degeneration of mammal SC during evolution, compared with other vertebrates. Based on our spatial data, we estimated the expression scores of top DEGs from these *FOXP1+* cells among different levels and found they were mainly enriched in *Imc*, which is one of the key nucleus isthmi for sensory processing in birds^{56,64} (Figure 4H). Consequently, we hypothesized that group 1 EXN, particularly those marked by *FOXP1* expression, were essential for OT to exert its functional capabilities. These findings provided further support for the potential functional convergent evolution between avian OT and specific regions of the mouse neocortex at a single-cell level.

Apart from the EXN, the development, and migration of INN has always been a hotspot in mammals,^{65,66} while in birds there is little knowledge of the origin of INN. Hence, we then extracted and identified 16 subclusters of INN within our data (Figures S5F and S5G). Based on the hierarchical clustering and the expression pattern of mammalian INN marker genes, we defined two main origins of the INN in OT: medial ganglionic eminence (MGE; INN_8/9/10/15/16), lateral ganglionic eminence (LGE; INN_0/1/2/3/5/6/7/11/12)⁵¹ (Figure S5H). However, there were three clusters of INN (INN_4/13/14) that could not be classified based on known markers of mammals and they were on the same branch of the clustering tree (Figure S5H). We further found these INN highly expressed the synuclein gamma (*SNCG*) and neuritin 1 (*NRN1*) (Figure S5I), which may play a different role in the OT and were a population of bird-unique INN in OT compared with mammals.

In summary, our snRNA-seq data provided a new understanding of the OT and its underlying function mechanisms, which can be a support and supplement to the spatial data with a higher RNA capture rate. Here we primarily focused on the various EXN of avian dOT and identified a specific subgroup, denoted as "group 1" here, which is likely closely associated with signal processing within the dOT. Furthermore, within the group 1 cells, we found a population of EXN highly expressed *FOXP1*, which is a pan-telencephalic marker in mammals.⁶⁷ The presence of *FOXP1+* cells in avian OT may be associated with the considerable expansion happened in avian tectum. The high degree of transcriptional similarity between specific cell populations in the avian dOT and the mouse sensory cortex also suggested a potential case of convergent evolution among vertebrates in their perception of the surrounding environment.

DISCUSSION

OT or SC has been studied for over forty years, with an increasing number of studies unveiling its diverse functions.¹⁰ However, a comprehensive understanding of its molecular landscape at the cellular level has been lacking. Meanwhile, the precise functions and underlying mechanisms of avian OT remain inconclusive.⁴ Fortunately, advancements in technology have provided us with the means to deepen our understanding of this structure. By employing spatial omics and snRNA-seq techniques, we have generated a spatial landscape of the avian tectum and explored its cellular organization. Moreover, comparative analysis with mouse datasets has enabled us to uncover instances of functional convergent evolution in OT and gain insights into its multimodal functions.

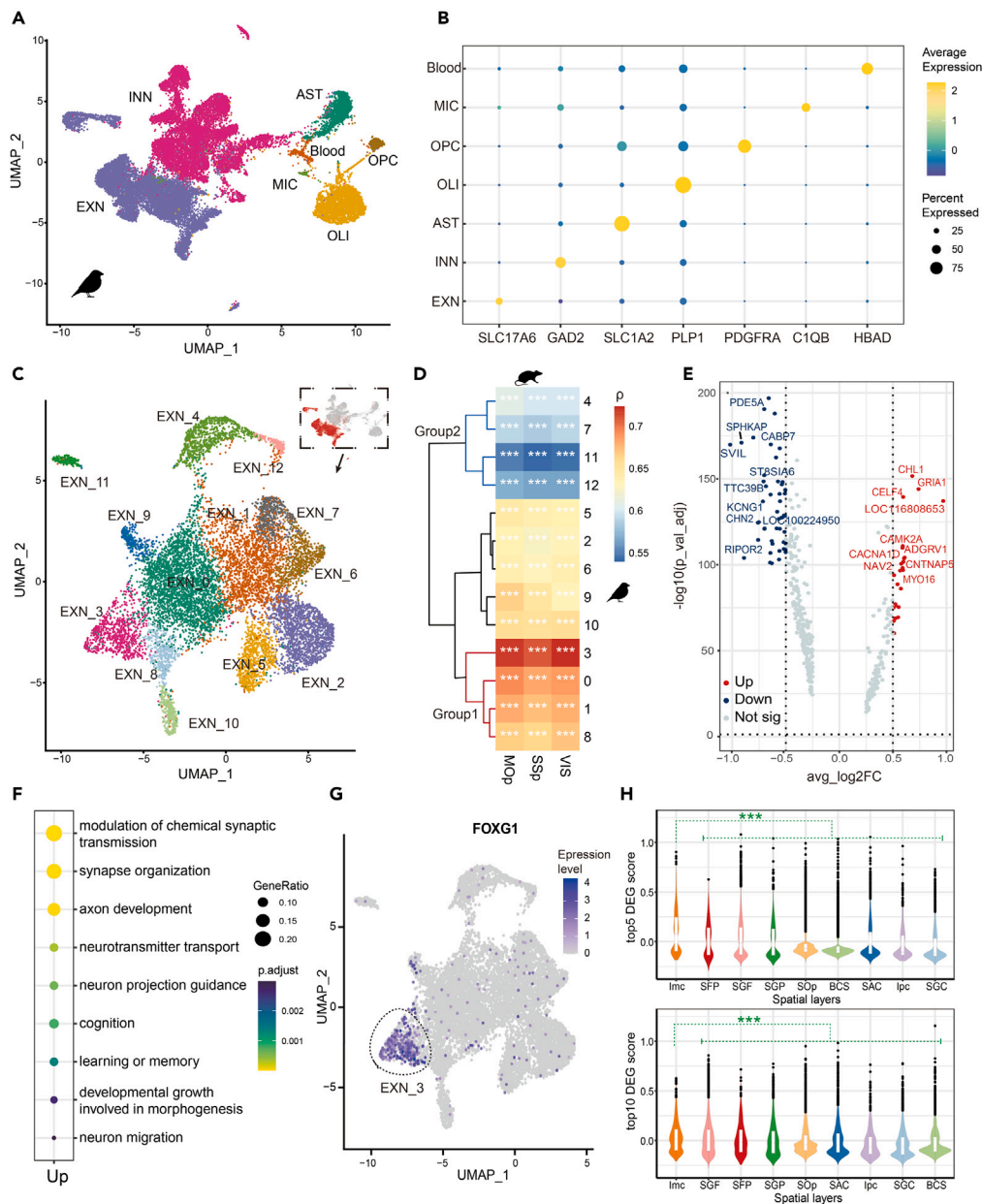


Figure 4. Single-nucleus atlas of the dOT (A) UMAP showing snRNA data of deeper layers from zebra finch OT

EXN, excitatory neurons; INN, inhibitory neurons; OLI, oligodendrocytes; AST, astrocytes; OPC, dendrocyte precursor cells; MIC, microglial cells; Blood, Blood cells.

(B) Dot plot of classic markers to identify cell types.

(C) Sub-clustering and further unsupervised clustering of EXN from snRNA data.

(D) Spearman correlations between scaled average expression profiles of avian subclusters and EXN from three brain regions of mice. VIS: visual area; SSp: primary somatosensory area; Mop: primary motor area; ***: p value < 0.001.

(E) Volcano plot showing the differentially expressed genes (DEGs) between group 1 and group 2 from D by Wilcoxon rank-sum test. The top 10 DEGs were annotated. The avg_log2FC represents average log2(fold change). Genes with adjusted p value < 0.05 and avg_log2FC>=0.5 are red (UP). Genes with adjusted p value < 0.05 and avg_log2FC<=-0.5 are blue (Down). Not sig: no significant genes.

(F) Dot plot showing enriched GO items of upregulated DEGs from group 1.

(G) Feature plot of FOXG1 in EXN.

(H) Violin plot of top 5 DEG score (Up) and top 10 DEG score (Down) of spatial layers. DEG was extracted from differential expression analysis of EXN_3 among all EXN. ***: p value<0.001, Wilcoxon rank-sum test.

Using Stereo-seq, here we reconstructed the layer structure of OT based on gene expression patterns, which align well with the corresponding anatomical structure and our ssDNA staining results (Figures 1B and 1C). We first reported the comprehensive layer-specific genes of avian OT, part of which has been implicated in the specialized functions previously documented, and these patterns existed in a high degree of conservation across avian species. These transcriptional atlases could help us acquire a deeper insight into avian OT. Concerning the function of layers, we reported differentially enriched pathways of each layer and found the SGP possessed the most diverse functions, like fear response and associative learning (Figures S2 and 2C). And we tried to explain these functions at molecular levels, where we found the relatively high expression of *TAC1*, *PENK*, *CCK*, *NRXN1* etc. In addition to gene function analysis, the expression of neurotransmitter receptors and transporters shed light on the potential neural connections within OT. Various layers of OT seem to be able to receive signals from the lpc and other midbrain regions via Ach and 5-HT respectively. Taken together, our findings substantiated the complex functional abilities of OT in birds and proposed some potential molecular mechanisms inside it.

The detailed characterization of neuronal subtypes and their spatial distribution within the OT has remained unclear for a long time. In this work, we employed two parallel methods, cell segmentation on spatial data and snRNA-seq analysis, to explore the cellular organization of the OT (Figures 3 and 4). The spatial cellular map obtained through cell segmentation revealed the distribution of neuronal and non-neuronal cells within the avian OT. Notably, in the avian OT, different subtypes of INN still have a well-layered distribution, a feature that is not possessed by SC in mice. Meanwhile, our snRNA-seq data identified an EXN population marked by *FOXG1* within dOT, which exhibited a high similarity to the EXN from the mouse neocortex. The *FOXG1*+ EXN in mammals has been reported to participate in forebrain expansion and higher cognitive functions.^{68,69} In our study, we observed that this specific EXN subtype may play a crucial role in higher-order processing functions within the OT. As for INN, the INN migration has not been well studied in birds, especially in OT. To explore the origin of INN in OT, we utilized classic INN markers from the mouse brain as a reference. Our findings indicated that LGE and MGE may be the main origins of INN in avian OT.

The understanding of the sensory processing and perception has always been a captivating topic for research, while our current understanding of it is still limited. One notable aspect lies in the evolutionary development of two visual pathways in vertebrates: the retinotectal (or tectofugal) pathway and the retinogeniculate (or thalamofugal) pathway.⁷⁰ In mammals, particularly primates, the majority of visual stimuli from the retina travel to the lateral geniculate nucleus in the thalamus, then to V1 in the neocortex, with only a few inputs directed to the SC.⁷¹ In contrast, birds, reptiles, and more primitive animals predominantly route almost all visual inputs to the OT, followed by higher-level analysis regions.⁴⁶ To date, comprehensive research addressing this significant transformation and elucidating its driving factors remains notably scarce. In this work, our data and analysis provided a new perspective for this process by focusing on the OT of birds, renowned for possessing exceptional vision and serving as a crucial node in evolutionary studies. These findings could not only contribute to our understanding of the architecture and innovation of avian OT but also establish a foundational dataset and knowledge base for future research on sensory evolution. Moreover, through a cross-species comparison between birds and mammals, our insights hint at the potential convergent evolution of multi-sensory processing in vertebrates.

Limitations of the study

However, the study is constrained by the limited availability of high-quality SC or OT data for other species, like primates and reptiles, preventing a comprehensive understanding of the primary factors driving the conversion of visual pathways in vertebrates. Consequently, further investigations are imperative to delve into the molecular and cellular changes occurring in sensory pathways across various species during evolution. Besides, limited by the capture capacity of current spatial sequencing technology and the relatively small size of avian brain cells, the cellular analysis of zebra finch spatial sections was hindered in this work. And the sample from different stages of development was also advised in the future research to further explore the conservation and innovation that existed in visual evolution of vertebrates.

STAR★METHODS

Detailed methods are provided in the online version of this paper and include the following:

- [KEY RESOURCES TABLE](#)
- [RESOURCE AVAILABILITY](#)
 - Lead contact
 - Materials availability
 - Data and code availability
- [EXPERIMENTAL MODEL AND STUDY PARTICIPANT DETAILS](#)
 - Animal care
- [METHOD DETAILS](#)
 - Brain tissue collection
 - Spatial section preparation and sequencing
 - Stereo-seq raw data processing
 - Single-nucleus suspension preparation
- [SNRNA-SEQ RAW DATA PROCESSING](#)
 - Spatial clustering and annotation

- Spatial sections integration and clustering
- Layer-specific expressed genes detection
- Correlation between pigeon and zebra finch
- Gene ontology enrichment analysis
- Gene module score of classic neurotransmitters
- Image-based single-cell segmentation and clustering
- Cell clustering and cell-type identification of snRNA-seq data
- The correlation of excitatory neurons from zebra finches and mice
- Top DEG score of spatial layers
- **QUANTIFICATION AND STATISTICAL ANALYSIS**

SUPPLEMENTAL INFORMATION

Supplemental information can be found online at <https://doi.org/10.1016/j.isci.2024.109009>.

ACKNOWLEDGMENTS

This work was supported by National Key Research and Development Program (No.2022YEF0203200). We sincerely thank the China National GeneBank for providing technical support. The cartoon plots of pigeon and zebra finch used in [Figure 1A](#) were collected from Alamy (<https://www.alamy.com/>) and VectorStock (<https://www.vectorstock.com/>), respectively.

AUTHOR CONTRIBUTIONS

Z.Z., S.L., and K.L. conceived and designed the study. K.L. wrote the manuscript and Z.Z., Y.L., D.C., S.L., and K.L. contributed to the discussion and revision of the manuscript. Zhenlong W., M.H., W.X., Zishi W., L.Y., and X.T. contributed to sample collection. Z.Z., S.L., and Zhenlong W. participated in guiding and providing suggestions for the study. K.L., Y.X., F.H., and P.L. provided technical support and conducted data analysis. All authors read and approved the final manuscript.

DECLARATION OF INTERESTS

The authors declare no competing interests.

Received: September 30, 2023

Revised: December 19, 2023

Accepted: January 22, 2024

Published: January 26, 2024

REFERENCES

1. Cang, J., Savier, E., Barchini, J., and Liu, X. (2018). Visual Function, Organization, and Development of the Mouse Superior Colliculus. *Annu. Rev. Vis. Sci.* 4, 239–262. <https://doi.org/10.1146/annurev-vision-091517-034142>.
2. Wurtz, R.H., and Albano, J.E. (1980). Visual-motor function of the primate superior colliculus. *Annu. Rev. Neurosci.* 3, 189–226. <https://doi.org/10.1146/annurev.ne.03.030180.001201>.
3. Basso, M.A., Bickford, M.E., and Cang, J. (2021). Unraveling circuits of visual perception and cognition through the superior colliculus. *Neuron* 109, 918–937. <https://doi.org/10.1016/j.neuron.2021.01.013>.
4. Liu, X., Huang, H., Snutch, T.P., Cao, P., Wang, L., and Wang, F. (2022). The Superior Colliculus: Cell Types, Connectivity, and Behavior. *Neurosci. Bull.* 38, 1519–1540. <https://doi.org/10.1007/s12264-022-00858-1>.
5. Knudsen, E.I., and Brainard, M.S. (1991). Visual instruction of the neural map of auditory space in the developing optic tectum. *Science* 253, 85–87. <https://doi.org/10.1126/science.2063209>.
6. Knudsen, E.I. (1982). Auditory and visual maps of space in the optic tectum of the owl. *J. Neurosci.* 2, 1177–1194. <https://doi.org/10.1523/JNEUROSCI.02-09-01177.1982>.
7. Isa, T., Marquez-Legorreta, E., Grillner, S., and Scott, E.K. (2021). The tectum/superior colliculus as the vertebrate solution for spatial sensory integration and action. *Curr. Biol.* 31, R741–R762. <https://doi.org/10.1016/j.cub.2021.04.001>.
8. Gutiérrez-Ibáñez, C., Iwaniuk, A.N., Moore, B.A., Fernández-Juricic, E., Corfield, J.R., Krilow, J.M., Kolominsky, J., and Wylie, D.R. (2014). Mosaic and concerted evolution in the visual system of birds. *PLoS One* 9, e90102. <https://doi.org/10.1371/journal.pone.0090102>.
9. White, B.J., Berg, D.J., Kan, J.Y., Marino, R.A., Itti, L., and Munoz, D.P. (2017). Superior colliculus neurons encode a visual saliency map during free viewing of natural dynamic video. *Nat. Commun.* 8, 14263. <https://doi.org/10.1038/ncomms14263>.
10. Basso, M.A., and May, P.J. (2017). Circuits for Action and Cognition: A View from the Superior Colliculus. *Annu. Rev. Vis. Sci.* 3, 197–226. <https://doi.org/10.1146/annurev-vision-102016-061234>.
11. Kardamakis, A.A., Pérez-Fernández, J., and Grillner, S. (2016). Spatiotemporal interplay between multisensory excitation and recruited inhibition in the lamprey optic tectum. *Elife* 5, e16472. <https://doi.org/10.7554/eLife.16472>.
12. Northmore, D. (2009). The Optic Tectum. In *Encyclopedia of Fish Physiology: From Genome to Environment*, 1Encyclopedia of Fish Physiology: From Genome to Environment, pp. 131–142. <https://doi.org/10.1002/0471733849.ch18>.
13. LaVail, J.H., and Cowan, W.M. (1971). The development of the chick optic tectum. I. Normal morphology and cytoarchitectonic development. *Brain Res.* 28, 391–419. [https://doi.org/10.1016/0006-8993\(71\)90053-9](https://doi.org/10.1016/0006-8993(71)90053-9).
14. Zhaoping, L. (2016). From the optic tectum to the primary visual cortex: migration through evolution of the saliency map for exogenous attentional guidance. *Curr. Opin. Neurobiol.* 40, 94–102. <https://doi.org/10.1016/j.conb.2016.06.017>.
15. Krauzlis, R.J., Bogadhi, A.R., Herman, J.P., and Bollimunta, A. (2018). Selective attention without a neocortex. *Cortex* 102, 161–175. <https://doi.org/10.1016/j.cortex.2017.08.026>.
16. Hafed, Z.M., Hoffmann, K.P., Chen, C.Y., and Bogadhi, A.R. (2023). Visual Functions of the Primate Superior Colliculus. *Annu. Rev. Vis. Sci.* 9, 361–383. <https://doi.org/10.1146/annurev-vision-111022-123817>.

17. Isa, T. (2002). Intrinsic processing in the mammalian superior colliculus. *Curr. Opin. Neurobiol.* 12, 668–677. [https://doi.org/10.1016/s0959-4388\(02\)00387-2](https://doi.org/10.1016/s0959-4388(02)00387-2).
18. Del Bene, F., Wyart, C., Robles, E., Tran, A., Looger, L., Scott, E.K., Isacoff, E.Y., and Baier, H. (2010). Filtering of visual information in the tectum by an identified neural circuit. *Science* 330, 669–673. <https://doi.org/10.1126/science.1192949>.
19. Wild, J.M., and Gaede, A.H. (2016). Second tectofugal pathway in a songbird (*Taeniopygia guttata*) revisited: Tectal and lateral pontine projections to the posterior thalamus, thence to the intermediate nidopallium. *J. Comp. Neurol.* 524, 963–985. <https://doi.org/10.1002/cne.23886>.
20. Chen, A., Liao, S., Cheng, M., Ma, K., Wu, L., Lai, Y., Qiu, X., Yang, J., Xu, J., Hao, S., et al. (2022). Spatiotemporal transcriptomic atlas of mouse organogenesis using DNA nanoball-patterned arrays. *Cell* 185, 1777–1792.e21. <https://doi.org/10.1016/j.cell.2022.04.003>.
21. Hu, J., Li, X., Coleman, K., Schroeder, A., Ma, N., Irwin, D.J., Lee, E.B., Shinohara, R.T., and Li, M. (2021). SpaGCN: Integrating gene expression, spatial location and histology to identify spatial domains and spatially variable genes by graph convolutional network. *Nat. Methods* 18, 1342–1351. <https://doi.org/10.1038/s41592-021-01255-8>.
22. Conlee, J.W., and Parks, T.N. (1986). Origin of ascending auditory projections to the nucleus mesencephalicus lateralis pars dorsalis in the chicken. *Brain Res.* 367, 96–113. [https://doi.org/10.1016/0006-8993\(86\)91583-0](https://doi.org/10.1016/0006-8993(86)91583-0).
23. Hao, Y., Hao, S., Andersen-Nissen, E., Mauck, W.M., 3rd, Zheng, S., Butler, A., Lee, M.J., Wilk, A.J., Darby, C., Zager, M., et al. (2021). Integrated analysis of multimodal single-cell data. *Cell* 184, 3573–3587.e29. <https://doi.org/10.1016/j.cell.2021.04.048>.
24. Hirai, H., Pang, Z., Bao, D., Miyazaki, T., Li, L., Miura, E., Parris, J., Rong, Y., Watanabe, M., Yuzaki, M., and Morgan, J.I. (2005). Cbln1 is essential for synaptic integrity and plasticity in the cerebellum. *Nat. Neurosci.* 8, 1534–1541. <https://doi.org/10.1038/nn1576>.
25. Shibata, M., Pattabiraman, K., Muchnik, S.K., Kaur, N., Morozov, Y.M., Cheng, X., Waxman, S.G., and Sestan, N. (2021). Hominini-specific regulation of CBLN2 increases prefrontal spinogenesis. *Nature* 598, 489–494. <https://doi.org/10.1038/s41586-021-03952-y>.
26. Rogers, J.H. (1987). Calretinin: a gene for a novel calcium-binding protein expressed principally in neurons. *J. Cell Biol.* 105, 1343–1353. <https://doi.org/10.1083/jcb.105.3.1343>.
27. Sinha, R., Lee, A., Rieke, F., and Haeseleer, F. (2016). Lack of CaBP1/Caldendrin or CaBP2 Leads to Altered Ganglion Cell Responses. *eNeuro* 3, ENEURO.0099-16.2016. <https://doi.org/10.1523/ENEURO.0099-16.2016>.
28. Mortensen, L.S., Park, S.J.H., Ke, J.B., Cooper, B.H., Zhang, L., Imig, C., Löwel, S., Reim, K., Brose, N., Demb, J.B., et al. (2016). Complexin 3 Increases the Fidelity of Signaling in a Retinal Circuit by Regulating Exocytosis at Ribbon Synapses. *Cell Rep.* 15, 2239–2250. <https://doi.org/10.1016/j.celrep.2016.05.012>.
29. Fleming, M.S., Ramos, D., Han, S.B., Zhao, J., Son, Y.J., and Luo, W. (2012). The majority of dorsal spinal cord gastrin releasing peptide is synthesized locally whereas neuromedin B is highly expressed in pain- and itch-sensing somatosensory neurons. *Mol. Pain* 8, 52. <https://doi.org/10.1186/1744-8069-8-52>.
30. Ohki-Hamazaki, H. (2000). Neuromedin B. *Prog. Neurobiol.* 62, 297–312. [https://doi.org/10.1016/s0301-0082\(00\)00004-6](https://doi.org/10.1016/s0301-0082(00)00004-6).
31. Clineschmidt, B.V., McGuffin, J.C., and Bunting, P.B. (1979). Neurotensin: antinociceptive action in rodents. *Eur. J. Pharmacol.* 54, 129–139. [https://doi.org/10.1016/0014-2999\(79\)90415-1](https://doi.org/10.1016/0014-2999(79)90415-1).
32. Russell, G., and Lightman, S. (2019). The human stress response. *Nat. Rev. Endocrinol.* 15, 525–534. <https://doi.org/10.1038/s41574-019-0228-0>.
33. Trainor, B.C. (2011). Stress responses and the mesolimbic dopamine system: social contexts and sex differences. *Horm. Behav.* 60, 457–469. <https://doi.org/10.1016/j.yhbeh.2011.08.013>.
34. Jukkola, T., Lahti, L., Naserke, T., Wurst, W., and Partanen, J. (2006). FGF regulated gene-expression and neuronal differentiation in the developing midbrain-hindbrain region. *Dev. Biol.* 297, 141–157. <https://doi.org/10.1016/j.ydbio.2006.05.002>.
35. Li, L., Ho, P.W.L., Liu, H., Pang, S.Y.Y., Chang, E.E.S., Choi, Z.Y.K., Malki, Y., Kung, M.H.W., Ramsden, D.B., and Ho, S.L. (2022). Transcriptional Regulation of the Synaptic Vesicle Protein Synaptogyrin-3 (SYNGR3) Gene: The Effects of NURR1 on Its Expression. *Int. J. Mol. Sci.* 23, 3646. <https://doi.org/10.3390/ijms23073646>.
36. Mulligan, M.K., Wang, X., Adler, A.L., Mozhui, K., Lu, L., and Williams, R.W. (2012). Complex control of GABA(A) receptor subunit mRNA expression: variation, covariation, and genetic regulation. *PLoS One* 7, e34586. <https://doi.org/10.1371/journal.pone.0034586>.
37. O'Rourke, T., and Boeckx, C. (2020). Glutamate receptors in domestication and modern human evolution. *Neurosci. Biobehav. Rev.* 108, 341–357. <https://doi.org/10.1016/j.neubiorev.2019.10.004>.
38. Meixner, M., Atanasova, S., Padberg, W., and Grau, V. (2014). Expression of acetylcholine receptors by experimental rat renal allografts. *BioMed Res. Int.* 2014, 289656. <https://doi.org/10.1155/2014/289656>.
39. Knott, E.L., and Leidenheimer, N.J. (2020). A Targeted Bioinformatics Assessment of Adrenocortical Carcinoma Reveals Prognostic Implications of GABA System Gene Expression. *Int. J. Mol. Sci.* 21, 8485. <https://doi.org/10.3390/ijms21228485>.
40. Veldic, M., Millischer, V., Port, J.D., Ho, A.M.C., Jia, Y.F., Geske, J.R., Biernacka, J.M., Backlund, L., McElroy, S.L., Bond, D.J., et al. (2019). Genetic variant in SLC1A2 is associated with elevated anterior cingulate cortex glutamate and lifetime history of rapid cycling. *Transl. Psychiatry* 9, 149. <https://doi.org/10.1038/s41398-019-0483-9>.
41. Bhat, S., El-Kasaby, A., Freissmuth, M., and Susic, S. (2021). Functional and Biochemical Consequences of Disease Variants in Neurotransmitter Transporters: A Special Emphasis on Folding and Trafficking Deficits. *Pharmacol. Ther.* 222, 107785. <https://doi.org/10.1016/j.pharmthera.2020.107785>.
42. O'Grady, G.L., Verschuuren, C., Yuen, M., Webster, R., Menezes, M., Fock, J.M., Pride, N., Best, H.A., Benavides Damm, T., Turner, C., et al. (2016). Variants in SLC18A3, vesicular acetylcholine transporter, cause congenital myasthenic syndrome. *Neurology* 87, 1442–1448. <https://doi.org/10.1212/WNL.0000000000003179>.
43. Chen, A., Sun, Y., Lei, Y., Li, C., Liao, S., Liang, Z., Lin, F., Yuan, N., Li, M., Wang, K., et al. (2022). Global Spatial Transcriptome of Macaque Brain at Single-Cell Resolution. Preprint at bioRxiv 1. <https://doi.org/10.1101/2022.03.23.485448>.
44. Veenman, C.L., and Reiner, A. (1994). The distribution of GABA-containing perikarya, fibers, and terminals in the forebrain and midbrain of pigeons, with particular reference to the basal ganglia and its projection targets. *J. Comp. Neurol.* 339, 209–250. <https://doi.org/10.1002/cne.903390205>.
45. Fujita, T., Aoki, N., Mori, C., Fujita, E., Matsushima, T., Homma, K.J., and Yamaguchi, S. (2021). Serotonergic Neurons in the Chick Brainstem Express Various Serotonin Receptor Subfamily Genes. *Front. Physiol.* 12, 815997. <https://doi.org/10.3389/fphys.2021.815997>.
46. Hellmann, B., Manns, M., and Güntürkün, O. (2001). Nucleus isthmi, pars semilunaris as a key component of the tectofugal visual system in pigeons. *J. Comp. Neurol.* 436, 153–166. <https://doi.org/10.1002/cne.1058>.
47. Asadollahi, A., Mysore, S.P., and Knudsen, E.I. (2010). Stimulus-driven competition in a cholinergic midbrain nucleus. *Nat. Neurosci.* 13, 889–895. <https://doi.org/10.1038/nn.2573>.
48. Noudoost, B., and Moore, T. (2011). The role of neuromodulators in selective attention. *Trends Cogn. Sci.* 15, 585–591. <https://doi.org/10.1016/j.tics.2011.10.006>.
49. Lei, Y., Cheng, M., Li, Z., Zhuang, Z., Wu, L., Sun, Y., Han, L., Huang, Z., Wang, Y., Wang, Z., et al. (2022). Spatially resolved gene regulatory and disease-related vulnerability map of the adult Macaque cortex. *Nat. Commun.* 13, 6747. <https://doi.org/10.1038/s41467-022-34413-3>.
50. Qiu, X., Zhu, D.Y., Yao, J., Jing, Z., Zuo, L., Wang, M., Min, K.H.J., Pan, H., Wang, S., Liao, S., et al. (2022). Spateo: multidimensional spatiotemporal modeling of single-cell spatial transcriptomics. Preprint at bioRxiv 1. <https://doi.org/10.1101/2022.12.07.519417>.
51. Colquitt, B.M., Merullo, D.P., Konopka, G., Roberts, T.F., and Brainard, M.S. (2021). Cellular transcriptomics reveals evolutionary identities of songbird vocal circuits. *Science* 371, eabd9704. <https://doi.org/10.1126/science.abd9704>.
52. Neveu, A.A., Zemel, B.M., Friedrich, S.R., von Gersdorff, H., and Mello, C.V. (2023). Cell type specializations of the vocal-motor cortex in songbirds. *Cell Rep.* 42, 113344. <https://doi.org/10.1016/j.celrep.2023.113344>.
53. Chen, A., Sun, Y., Lei, Y., Li, C., Liao, S., Meng, J., Bai, Y., Liu, Z., Liang, Z., Zhu, Z., et al. (2023). Single-cell spatial transcriptome reveals cell-type organization in the macaque cortex. *Cell* 186, 3726–3743.e24. <https://doi.org/10.1016/j.cell.2023.06.009>.
54. Olkowicz, S., Kocourek, M., Lučan, R.K., Porteš, M., Fitch, W.T., Herculano-Houzel, S., and Nêmec, P. (2016). Birds have primate-like numbers of neurons in the forebrain. *Proc. Natl. Acad. Sci. USA* 113, 7255–7260. <https://doi.org/10.1073/pnas.1517131113>.
55. Falcone, C. (2022). Evolution of astrocytes: From invertebrates to vertebrates. *Front. Cell Dev. Biol.* 10, 931311. <https://doi.org/10.3389/fcell.2022.931311>.
56. Wang, Y., Major, D.E., and Karten, H.J. (2004). Morphology and connections of nucleus isthmi pars magnocellularis in chicks (*Gallus gallus*). *J. Comp. Neurol.* 469, 275–297. <https://doi.org/10.1002/cne.11007>.
57. Panksepp, J., Burgdorf, J., Beinfeld, M.C., Kroes, R.A., and Moskal, J.R. (2004). Regional

- brain cholecystokinin changes as a function of friendly and aggressive social interactions in rats. *Brain Res.* 1025, 75–84. <https://doi.org/10.1016/j.brainres.2004.07.076>.
58. Peyon, P., Saied, H., Lin, X., and Peter, R.E. (1999). Postprandial, seasonal and sexual variations in cholecystokinin gene expression in goldfish brain. *Brain Res.* 74, 190–196. [https://doi.org/10.1016/s0169-328x\(99\)00282-x](https://doi.org/10.1016/s0169-328x(99)00282-x).
 59. Manns, M., and Güntürkün, O. (2003). Light experience induces differential asymmetry pattern of GABA- and parvalbumin-positive cells in the pigeon's visual midbrain. *J. Chem. Neuroanat.* 25, 249–259. [https://doi.org/10.1016/s0891-0618\(03\)00035-8](https://doi.org/10.1016/s0891-0618(03)00035-8).
 60. Shi, H., He, Y., Zhou, Y., Huang, J., Wang, B., Tang, Z., Tan, P., Wu, M., Lin, Z., Ren, J., et al. (2022). Spatial Atlas of the Mouse Central Nervous System at Molecular Resolution. Preprint at bioRxiv 1. <https://doi.org/10.1101/2022.06.20.496914>.
 61. Knapp, J.E., Oliveira, M.A., Xie, Q., Ernst, S.R., Riggs, A.F., and Hackert, M.L. (1999). The structural and functional analysis of the hemoglobin D component from chicken. *J. Biol. Chem.* 274, 6411–6420. <https://doi.org/10.1074/jbc.274.10.6411>.
 62. Yao, Z., van Velthoven, C.T.J., Nguyen, T.N., Goldy, J., Sedeno-Cortes, A.E., Baftizadeh, F., Bertagnoli, D., Casper, T., Chiang, M., Crichton, K., et al. (2021). A taxonomy of transcriptomic cell types across the isocortex and hippocampal formation. *Cell* 184, 3222–3241.e26. <https://doi.org/10.1016/j.cell.2021.04.021>.
 63. Kumamoto, T., and Hanashima, C. (2017). Evolutionary conservation and conversion of Foxg1 function in brain development. *Dev. Growth Differ.* 59, 258–269. <https://doi.org/10.1111/dgd.12367>.
 64. Wang, S.R. (2003). The nucleus isthmi and dual modulation of the receptive field of tectal neurons in non-mammals. *Brain Res. Brain Res. Rev.* 41, 13–25. [https://doi.org/10.1016/s0165-0173\(02\)00217-5](https://doi.org/10.1016/s0165-0173(02)00217-5).
 65. Schmitz, M.T., Sandoval, K., Chen, C.P., Mostajo-Radji, M.A., Seeley, W.W., Nowakowski, T.J., Ye, C.J., Paredes, M.F., and Pollen, A.A. (2022). The development and evolution of inhibitory neurons in primate cerebrum. *Nature* 603, 871–877. <https://doi.org/10.1038/s41586-022-04510-w>.
 66. Zhao, Z., Zhang, D., Yang, F., Xu, M., Zhao, S., Pan, T., Liu, C., Liu, Y., Wu, Q., Tu, Q., et al. (2022). Evolutionarily conservative and non-conservative regulatory networks during primate interneuron development revealed by single-cell RNA and ATAC sequencing. *Cell Res.* 32, 425–436. <https://doi.org/10.1038/s41422-022-00635-9>.
 67. Tao, W., and Lai, E. (1992). Telencephalon-restricted expression of BF-1, a new member of the HNF-3/fork head gene family, in the developing rat brain. *Neuron* 8, 957–966. [https://doi.org/10.1016/0896-6273\(92\)90210-5](https://doi.org/10.1016/0896-6273(92)90210-5).
 68. Liu, J., Yang, M., Su, M., Liu, B., Zhou, K., Sun, C., Ba, R., Yu, B., Zhang, B., Zhang, Z., et al. (2022). FOXG1 sequentially orchestrates subtype specification of postmitotic cortical projection neurons. *Sci. Adv.* 8, eabh3568. <https://doi.org/10.1126/sciadv.abh3568>.
 69. Mariani, J., Coppola, G., Zhang, P., Abyzov, A., Provini, L., Tomasini, L., Amenduni, M., Szekeley, A., Palejev, D., Wilson, M., et al. (2015). FOXG1-Dependent Dysregulation of GABA/Glutamate Neuron Differentiation in Autism Spectrum Disorders. *Cell* 162, 375–390. <https://doi.org/10.1016/j.cell.2015.06.034>.
 70. Knudsen, E.I. (2020). Evolution of neural processing for visual perception in vertebrates. *J. Comp. Neurol.* 528, 2888–2901. <https://doi.org/10.1002/cne.24871>.
 71. Ghodrati, M., Khaligh-Razavi, S.M., and Lehky, S.R. (2017). Towards building a more complex view of the lateral geniculate nucleus: Recent advances in understanding its role. *Prog. Neurobiol.* 156, 214–255. <https://doi.org/10.1016/j.pneurobio.2017.06.002>.
 72. Guo, X., Chen, F., Gao, F., Li, L., Liu, K., You, L., Hua, C., Yang, F., Liu, W., Peng, C., et al. (2020). CNSA: a data repository for archiving omics data. *Database (Oxford)* 2020, baaa055. <https://doi.org/10.1093/database/baaa055>.
 73. Chen, F.Z., You, L.J., Yang, F., Wang, L.N., Guo, X.Q., Gao, F., Hua, C., Tan, C., Fang, L., Shan, R.Q., et al. (2020). CNGBdb: China National GeneBank DataBase. *Yi Chuan* 42, 799–809. <https://doi.org/10.16288/j.ycz.20-080>.
 74. Dobin, A., Davis, C.A., Schlesinger, F., Drenkow, J., Zaleski, C., Jha, S., Batut, P., Chaisson, M., and Gingeras, T.R. (2013). STAR: ultrafast universal RNA-seq aligner. *Bioinformatics* 29, 15–21. <https://doi.org/10.1093/bioinformatics/bts635>.
 75. Bakken, T.E., Hodge, R.D., Miller, J.A., Yao, Z., Nguyen, T.N., Aevermann, B., Barkan, E., Bertagnoli, D., Casper, T., Dee, N., et al. (2018). Single-nucleus and single-cell transcriptomes compared in matched cortical cell types. *PLoS One* 13, e0209648. <https://doi.org/10.1371/journal.pone.0209648>.
 76. Chuanyu Liu, T.W., Fan, Y.L., Wu, L., Junkin, M., Wang, Z., Yu, Y., Wang, W., Wei, W., Yue, Y., Wang, M., et al. (2019). A portable and cost-effective microfluidic system for massively parallel single-cell transcriptome profiling. Preprint at bioRxiv 1. <https://doi.org/10.1101/818450>.
 77. Wu, T., Hu, E., Xu, S., Chen, M., Guo, P., Dai, Z., Feng, T., Zhou, L., Tang, W., Zhan, L., et al. (2021). clusterProfiler 4.0: A universal enrichment tool for interpreting omics data. *Innovation* 2, 100141. <https://doi.org/10.1016/j.xinn.2021.100141>.

STAR★METHODS

KEY RESOURCES TABLE

REAGENT or RESOURCE	SOURCE	IDENTIFIER
Biological samples		
#1 Rock pigeon (male, 12-month-old)	This study	N/A
#2 Zebra finch (female, 12-month-old)	This study	N/A
#3 Zebra finch (male, 12-month-old)	This study	N/A
#4 Zebra finch (female, 12-month-old)	This study	N/A
#5 Zebra finch (female, 12-month-old)	This study	N/A
Chemicals, peptides, and recombinant proteins		
Normal Goat Serum Blocking Solution	Vector Lab	S-1000-20
Nucleic Acid Dye	Thermo	Cat#Q10212
Qubit™ dsDNA Assay Kit	Thermo	Cat#Q10212
RNase inhibitor	NEB	M0314L
blocking buffer	Roche	Cat#11096176001
RNase A	Sigma	Cat#R4642
MgCl ₂	Ambion	AM9530G
T4 ligase	NEB	Cat#M0202V
Tissue-Tek OCT	Sakura	Cat#4583
Deposited data		
Public <i>in situ</i> hybridization image data	https://portal.brain-map.org/	N/A
Public mouse isocortex single cell transcriptomic data	NeMO Archive	nemo:dat-jb2f34y
Public mouse spatial transcriptomic data	Single Cell Portal	SCP1830
snRNA data of zebra finches and rock pigeons	This study	https://db.cngb.org/search/project/CNP0004708/
Stereo-seq data of avian optic tectum	This study	https://db.cngb.org/stomics/project/STT0000064
Codes for bioinformatic analysis	This study	https://github.com/Coleliao/Spatial_OT
Oligonucleotides		
Stereo-seq-TSO: CTGCTGACGTACTGAGAGGC/rG//rG//iXNA_G/	Sangon	N/A
cDNA PCR primer: CTGCTGACGTACTGAGAGGC	Sangon	N/A
Stereo-seq-library-F: /5phos/CTGCTGACGTACTGAGAGG*C*A	Sangon	N/A
Stereo-seq-library-R: GAGACGTTCTCGACTCAGCAGA	Sangon	N/A
Stereo-seq-library-splint-oligo: GTACGTCAGCAGGAGACGTTCTCG	Sangon	N/A
Stereo-seq-read1: CTGCTGACGTACTGAGAGGCATGGCGACCT TATCAG	Sangon	N/A
Stereo-seq-read2: GCCATGTCGTTCTGTGAGCCAAGGAGT	Sangon	N/A

(Continued on next page)

Continued

REAGENT or RESOURCE	SOURCE	IDENTIFIER
Stereo-seq-MDA-primer: TCTGCTGAGTCGAGAACGTC	Sangon	N/A
Software and algorithms		
SAW	https://github.com/BGIResearch/SAW	V2.1.0
STAR	https://github.com/alexdobin/STAR	V2.5.3
R	https://cran.r-project.org/	V4.2.0
Seurat	https://satijalab.org/seurat/	V4.3.0
SeuratDisk	https://github.com/mojaveazure/seurat-disk	V0.0.0.9020
psych	https://cran.r-project.org/web/packages/psych/	V2.2.5
clusterProfiler	http://www.bioconductor.org/packages/release/bioc/html/clusterProfiler.html	V4.2.2
ggplot2	https://cran.rstudio.com/web/packages/ggplot2/index.html	V3.3.6
ggpubr	https://cran.r-project.org/web/packages/ggpubr/index.html	V0.4.0
org.Hs.e.g.,.db	https://bioconductor.org/packages/release/data/annotation/html/org.Hs.e.g.db.html	V1.14.2
ComplexHeatmap	https://bioconductor.org/packages/release/bioc/html/ComplexHeatmap.html	V2.11.1
dplyr	https://cran.r-project.org/web/packages/dplyr/index.html	V1.0.10
python	https://www.python.org/	V3.9.0
Spateo	https://github.com/aristoteleo/spateo-release	V1.0.2
SpaGCN	https://github.com/jianhuupenn/SpaGCN	V1.2.7
pandas	https://pypi.org/project/pandas/	V2.0.3
numpy	https://pypi.org/project/numpy/	V1.24.0
scanpy	https://scanpy.readthedocs.io/en/stable/	V1.9.3
anndata	https://anndata.readthedocs.io/en/latest/	V0.9.2

RESOURCE AVAILABILITY**Lead contact**

Further information and requests for the resources and reagents may be directed to and will be fulfilled by the lead contact, Zhenkun Zhuang (zhuangzhenkun@genomics.cn).

Materials availability

All materials used for stereo-seq and snRNA-seq are commercially available.

Data and code availability

The snRNA data that support the findings of this study have been deposited into the CNGB Sequence Archive (CNSA)⁷² of China National GeneBank DataBase (CNGBdb)⁷³ with accession number CNP0004708 (<https://db.cngb.org/search/project/CNP0004708/>). The stereo-seq data of avian optic avian from zebra finches and rock pigeon used in this study can be accessed and downloaded via <https://db.cngb.org/stomics/project/STT0000064>. All data are publicly available as of the date of publication. The transcriptomic data and *in situ* hybridization data of mouse used in this study were previously published, and their accession numbers are listed in the [key resources table](#).

All data were analyzed with standard programs and packages, as detailed in the [key resources table](#). All original code used to analyze the data has been deposited at https://github.com/Coleliao/Spatial_OT and is publicly available.

Any additional information required to reanalyze the data reported in this paper is available from the [lead contact](#) upon request.

EXPERIMENTAL MODEL AND STUDY PARTICIPANT DETAILS

Animal care

The animal protocol was approved by the Institutional Review Board School, Zhengzhou University (ZZUIRB2022-23). Animal care complied with the guidelines of this committee. One pigeon (*Columba livia*) and four zebra finches (*Taeniopygia guttata*) used in this study were all healthy adults at 12 months of age. Section P1, P2, and P3 for Stereo-seq were from pigeon #1(male). Section Z1 and Z2 for Stereo-seq were from zebra finch #1 (female) and #2 (male) respectively. Samples for single nucleus sequencing were from zebra finch #3 (female) and #4 (male).

METHOD DETAILS

Brain tissue collection

Tissues were snap-frozen in liquid nitrogen prechilled isopentane in Tissue-Tek OCT (Sakura, 4583) and transferred to a -80°C freezer for storage before the experiment. Cryosections were cut at a thickness of 10 μm in a Leica CM1950 cryostat. Coronal segmentation was performed using a freezing microtome. For Section P1, P2, and P3 for Stereo-seq, sections were collected from the position at 12.0, 12.5, and 13.0 mm from the forebrain extremity along the anterior-to-posterior direction respectively. Section Z2 and Z1 of zebra finch were from positions at 6.0 and 6.5 mm from the forebrain extremity. The samples for snRNA-seq were punched out from the tissue under the SGF layer of zebra finch #3 and #4.

Spatial section preparation and sequencing

Stereo-seq experiment workflows were performed as previously described by Chen et al.²⁰ In brief, Tissue sections were adhered to the Stereo-seq chip surface and incubated at 37°C for 3–5 min. Subsequently, the sections underwent fixation in methanol for 40 min at -20°C before initiating the Stereo-seq library preparation. Before sequencing, the same sections were stained with a nucleic acid dye (Thermo fisher, #Q10212) to detect the ssDNA distribution, and imaging was conducted using a Ti-7 Nikon Eclipse microscope before capturing them *in situ* through the FITC channel. Following this, we performed *in situ* reverse transcription, amplification, library construction, and sequencing, adhering to the manufacturer's protocol.

Stereo-seq raw data processing

The fastq files from the Stereo-seq experiment underwent processing following a previously established workflow.²⁰ The initial reads in the Stereo-seq data included Coordinate Identity (CID) sequences, which were aligned to the predefined coordinates of the Stereo-seq chip obtained during the first round of sequencing. During this alignment process, a maximum of one base mismatch was allowed. Reads containing Molecular Identifiers (MID) with N bases or more than two bases with a quality score below 10 were excluded from the dataset. The CID and MID associated with each read were then added to the read header. The retained reads were subsequently aligned to the reference genome using STAR,⁷⁴ and reads with a mapping quality score greater than 10 were tallied and annotated to their respective genes. Unique Molecular Identifiers (UMIs) sharing the same CID and gene locus were merged into a single UMI, allowing for one mismatch to account for sequencing and PCR errors. This information was then used to generate an expression profile matrix containing CID information. The entire pipeline SAW can be accessed at <https://github.com/STOmics/SAW>. Notably, to improve the mapping of detected fragments to more annotated exonic and intronic regions, we generated a modified GTF annotation file based on bTaeGut1.4.pri from the National Center for Biotechnology Information (NCBI). Subsequently, the single-nucleus RNA-seq (snRNA-seq) data were aligned to the reference using STAR (v2.5.3) with the aforementioned modified GTF file.

Single-nucleus suspension preparation

A single-nucleus suspension was prepared following established procedures.⁷⁵ In brief, frozen brain tissue samples from birds were placed in a Dounce homogenizer containing 2 mL of pre-chilled homogenization buffer, and the homogenizer was kept on ice during the grinding process. The tissue was homogenized with 10–15 strokes using pestle A, followed by 10–15 strokes using pestle B. Subsequently, an additional 2 mL of homogenization buffer was added to the Dounce homogenizer, and the homogenate was filtered through 30 μm MACS Smart Strainers (Miltenyi Biotech, #130-110-915) into a 15 mL conical tube. The tube was then centrifuged at 500 g for 5 min at 4°C to pellet the nuclei. The resulting pellet was resuspended in 1.5 mL of blocking buffer and subjected to another centrifugation step at 500 g for 5 min at 4°C to pellet the nuclei once more. The isolated nuclei were subsequently resuspended in cell resuspension buffer for use in the subsequent single-nucleus RNA sequencing library preparation.

snRNA-seq library construction and sequencing

The DNBelab C Series High-throughput Single-Cell RNA Library Preparation Kit (MGI, #940-000047-00) was employed to construct sequencing libraries following the manufacturer's instructions. In summary, single-nucleus suspensions were used for various steps, including droplet generation, emulsion breakage, collection of beads, reverse transcription, second-strand synthesis, cDNA amplification, and amplification of droplet index products to generate barcoded libraries. The quantification of sequencing libraries was performed using the Qubit

ssDNA Assay Kit (Thermo Fisher Scientific, #Q10212), and the libraries were subsequently sequenced on the ultra-high-throughput DIPSEQ T1 or DIPSEQ T10 sequencers at the China National GeneBank (Shenzhen, China).

SNRNA-SEQ RAW DATA PROCESSING

The sequencing data were processed following the methods previously outlined.⁷⁶ Initially, bead barcodes and unique molecular identifier sequences were extracted using the 'parse' function available in PISA (<https://github.com/shiquan/PISA>). For cDNA libraries, the first 10–20 base pairs (bp) of 'read1' served as bead barcodes, the next 10 bp (21–30 bp) represented the UMI sequence, and the entire 'read2' (100 bp) was employed for downstream alignment analysis. In the case of Droplet Index libraries, the first 10–20 bp of 'read1' were designated as bead barcodes, the first 10 bp of 'read2' were considered the UMI sequence, and the subsequent 10 bp (11–20 bp) and 10 bp (21–30 bp) of 'read2' were designated as droplet index barcodes. Reads with incorrect barcodes, as per the barcode list, were excluded. Subsequently, the single-nucleus RNA-seq data were aligned to the genome reference using STAR (v2.5.3), with the previously mentioned modified GTF file. To determine the actual number of beads, the 'barcodeRanks' function from the DropletUtils tool was utilized to identify the threshold value representing a sharp transition in the distribution of total UMI counts. Beads with UMI counts below this threshold were discarded. Beads considered to belong to the same cell were merged, and gene expression in cells was quantified using PISA.

Spatial clustering and annotation

The reads captured by DNBs were summarized based on a binning method, which contained 100 × 100 single DNB in a bin100 (bin, 50 μm diameter). All bins of each section were clustered in SpaGCN (v1.2.7)²¹ separately. The average spatial position of all DNBs in one bin was set as the position of the bin, which was used in SpaGCN. Genes expressed in less than 3 bins were removed with function `spg.prefilter_genes()`. During spatial clustering by SpaGCN, parameters followed: $p = 0.5$, $n_clusters = 28$, $r_seed = t_seed = n_seed = 100$, and other parameters followed the official tutorial. The default clustering model of SpaGCN was used. The region annotation was based on both anatomical knowledge and unsupervised clustering results, and validated by corresponding ssDNA staining result of each section. All sections were clustered and manually annotated separately.

Spatial sections integration and clustering

To remove the batch effect, we integrated all sections in Seurat (v4.3.0).²³ Before integration, bins in any section in which genes captured less than 200 were filtered. Only the main regions of each section were extracted for subsequent analysis, which contained SOp, SGF, SGC, SAC, BCS, SGP, SFP, Imc, and lpc. Then 5 spatial sections were normalized and scaled by the function 'SCTransform' in Seurat. All sections were then integrated by 3,000 anchors with the mutual nearest neighbor (MNN) algorithm in Seurat. The dimensionality reduction and clustering of the integrated object were then achieved with functions 'RunPCA' and 'RunUMAP' with $dim = 1:30$ and $resolution = 1.0$. Other parameters in the clustering flow were default.

Layer-specific expressed genes detection

The differentially expressed genes (DEGs) of each domain in the avian OT were detected by the 'FindAllMarkers' function with the Wilcoxon rank-sum test. The normalized count matrix of the integrated object from two species was used for the differential expression calculation. Only genes with $\log_{2}(\text{threshold}) > 0.1$ during `FindAllMarkers()` were kept for further analysis. Genes with the adjusted p value less than 0.05, calculated by Bonferroni correction, were regarded as significant for each layer.

Correlation between pigeon and zebra finch

The bin data from two species was normalized by function `LogNormalize()` in Seurat with default parameters. Expression matrix from the same species but different sections was merged into one. The top 50 DEGs, of which adjusted p value less than 0.05, of all main tectum regions were selected. The average expression of each region for these selected genes was calculated by the 'AverageExpression' function on the data slot. Then the Spearman correlation was conducted in R with package `psych` (v2.2.5). The heatmap was visualized by `ComplexHeatmap` (v2.11.1).

Gene ontology enrichment analysis

The top 50 DEGs with the highest average fold change and adjusted p value less than 0.05 of each region in the OT were selected for the Gene Ontology (GO) enrichment analysis. Only DEGs that could be transferred into one-to-one orthologous genes of human were kept for further analysis. The GO analysis was conducted in R with a package named `clusterProfiler` (v4.2.2).⁷⁷ All genes were transformed into ENTREZ ID by the human genome reference 'org.Hs.e.g.,db'. The compared GO enrichment was performed by function 'compareCluster' with parameters: $ont = 'BP'$, $pAdjustMethod = 'BH'$, $pvalueCutoff = 0.05$, $qvalueCutoff = 0.05$. In addition, as for the SGP layer, we conducted the enrichment on its top 50 DEGs with the function 'enrichGO' with the same parameter above. Only GO items with a q value less than 0.05 were selected.

Gene module score of classic neurotransmitters

The integrated data was used for the module score with the function 'AddModuleScore' function in Seurat. Main neurotransmitter receptor types included in this work were: the γ -aminobutyric acid (GABA) receptors, glutamate receptors, monoamine receptors, where we only considered serotonin (5-Hydroxytryptamine, 5-HT), and acetylcholine receptors. The main neurotransmitter transporters included GABA transporters, glutamate transporters, monoamine transporters and acetylcholine transports. Only genes expressed in our sections were taken into account in the scoring. All detailed genes were listed in [Table S2](#). After scoring, the Kruskal-Wallis rank-sum test was conducted among scores of all regions in R by ggpubr (v0.4.0) to check the overall significance.

Image-based single-cell segmentation and clustering

To obtain the spatial data at cellular resolution, we only conducted cell segmentation on our spatial data. Due to the limited sequencing depth of current technology and the small size of birds compared with mammals, especially for zebra finch, the cell segmentation was conducted only on the Section P1 from pigeon and Section Z1 from zebra finch. The cell segmentation was performed by Spateo (v1.0.2)⁵⁰ in Python. We first identified the nucleus based on the ssDNA staining picture with a watershed-based approach. To expand the segmented cells from nuclei to cytoplasm, we then expanded each nucleus by 10 pixels and set the maximum area of each cell as 1,200 pixels. After the segmentation, for Section P1, we only extracted the OT area. Segmented cells with genes more than 150 and less than 2,500 were kept for further analysis. Since the average quality of segmented cells of Section Z1 was not qualified for further clustering and cell type annotation, in the following process, we only used P1 for the dimension reduction and unsupervised clustering, while the section from zebra finch was used for validation. The clustering of cells was conducted in Seurat (v4.3.0) with a default pipeline. All clusters were classified into seven major cell types based on the expression of markers.

Cell clustering and cell-type identification of snRNA-seq data

Basic processing and visualization of the snRNA-seq data were performed with Seurat (v4.3.0). All matrices were created Seurat object by function 'CreateSeuratObject' with parameters: min.cells = 3, min.features = 200. The data from the same sample but different libraries were merged. Nuclei with genes less than 300 or more than 3,000 were filtered out. After the quality control, 29,281 nuclei in total were finally remained for downstream analysis. We then integrated the snRNA-seq data from different samples in Seurat. The integration and clustering followed the same pipeline as the integration of spatial bin data before. Cell types were identified by classic markers reported in previous studies. In addition, after the major cell type annotation, we extracted and re-integrated the EXN and INN for further clustering.

The correlation of excitatory neurons from zebra finches and mice

We downloaded the single-cell sequencing data of the mouse brain and extracted three brain regions from the data, including VIS, SSp, and MOp.⁶² Only EXN from our snRNA data of birds and downloaded mouse data were kept. Considering the downloaded mouse data was too large, we down-sampled 30,000 cells for further correlation. 2,500 high variable genes (HVGs) across the bird data were calculated with the function 'FindVariableFeatures'. All mouse genes were converted into all caps for consistency. Only one-to-one orthologous HVGs existed both in mice and birds were used to calculate the average expression for each brain region and cell type. Then the Spearman correlation was conducted in R with package psych (v2.2.5). The hierarchical clustering of all cell types in deeper OT of zebra finch was based on the Spearman correlation coefficient.

Top DEG score of spatial layers

DEGs of EXN_3 were calculated by the function FindMarkers() in Seurat among all EXN subclusters. Only DEGs with adjusted p value < 0.05 and existed both in snRNA data and spatial RNA data were remained for further analysis. Top DEGs were selected by the order of fold change. The scores were calculated by function AddModuleScore() on integrated spatial data of five sections. All parameters followed the official tutorial of Seurat.

QUANTIFICATION AND STATISTICAL ANALYSIS

No statistical methods were used to predetermine sample sizes, but the sample sizes here are similar to those reported in previous publications. No randomization was used during data collection as there was a single experimental condition for all acquired data. Data collection and analyses were not performed blind to the conditions of the experiments as all experiments followed the same experimental condition. Statistical details of experiments and analyses can be found in the figure legends and main text above. All statistical tests were two-sided, and statistical significance was considered when p value < 0.05. To account for multiple-testing, the p values were adjusted using the Bonferroni correction.